3798 *Chem. Mater.* **2010,** *22,* 3798–3806
DOI:10.1021/cm903386c

CHEMISTRY OF MATERIALS
Article

Subnanoscale Lanthanum Distribution in Lanthanum-Incorporated Hafnium Oxide Thin Films Grown Using Atomic Layer Deposition

Tuo Wang and John G. Ekerdt*

Department of Chemical Engineering, The University of Texas at Austin, Austin, Texas 78712

Received November 5, 2009. Revised Manuscript Received March 9, 2010

The subnanoscale spatial distribution of La in La-incorporated HfO_2 thin films grown by atomic layer deposition (ALD) is characterized using angle resolved X-ray photoelectron spectroscopy (AR-XPS) and ellipsometry. The (La 3d)/(O 1s) photoelectron intensity ratios and film void fractions are acquired by conducting AR-XPS at small take off angles and processing the ellipsometry data through the effective medium approximation model. The existence of a $HfLa_xO_y-HfO_2-HfLa_xO_y$ structure is confirmed by AR-XPS. The ellipsometry data reveal an abrupt decrease of film void fraction after two HfO_2 growth cycles. More than two and less than three ALD HfO_2 layers interact with one ALD layer of La_2O_3 in such a way that the first two ALD HfO_2 layers mismatch with La_2O_3 and form a $HfO_2-La_2O_3$ mixture with a different structure compared to films with a third ALD HfO_2 layer that completes the formation of a continuous HfO_2 surface. At least four ALD HfO_2 layers are required for La free HfO_2 interval layers to exist in the film. This AR-XPS-ellipsometry method is potentially applicable to characterizing other amorphous ALD grown systems containing incorporated elements with subnanoscale variations.

1. Introduction

Atomic layer deposition (ALD) is a chemical vapor deposition technique based on self-terminating surface reactions, leading to highly controlled layer-by-layer growth of thin films at the atomic level.[1] In recent years, ALD has become a well-established technique to grow various inorganic thin film materials, including oxides, nitrides, sulphides, selenides, tellurides, pure elements, etc.[2] Because of the unique growth mechanism, ALD grown films can be extremely conformal. Because the precursors are separately supplied to the growth chamber, precursors with high reactivity can be used, enabling relatively low growth temperatures compared with other chemical film deposition techniques.

Incorporating another element is considered as one of the effective ways to modify the properties of a material, such as conductivity, dielectric constant, and crystallization temperature. In terms of ALD grown films, the incorporation can be achieved by repeatedly depositing two materials in alternating cycles, i.e., x ALD layers of the host material followed by one ALD layer of the incorporated material, which defines the incorporation level, and then repeating this sequence to achieve the desired film thickness. For example, Er has been incorporated into Y_2O_3 for optical applications.[3,4] In the field of high-k dielectrics, amorphizers and crystallizers have been added to HfO_2 to change material properties.[5] Specifically, Si, Al, and La have been incorporated into HfO_2 for the purpose of amorphous stabilization,[6−11] and Y has been incorporated to induce the cubic phase.[12]

However, the spatial distribution of the incorporated layer(s) in many ALD-grown systems remains unclear. Unlike homogeneous ternary systems grown by physical vapor deposition (PVD) or chemical vapor deposition (CVD), the incorporated material is more likely to be separated by the host material in an ALD film, thereby forming a layered periodic structure, especially when the ALD cycle ratio of the host material to the incorporated material is high. We have proposed that the existence of this periodic structure may add an extra advantage to stabilize the amorphous phase of high-k dielectric thin films after high temperature annealing.[10] For ALD-grown $HfAlO_x$, the films with similar composition but

*Corresponding author. E-mail: ekerdt@che.utexas.edu. Tel.: (512) 471-4689. Fax: (512) 471-7060.

(1) Suntola, T. *Thin Solid Films* **1992**, *216*(1), 84–89.
(2) Puurunen, R. L. *J. Appl. Phys.* **2005**, *97*(12), 121301/1–121301/52.
(3) Van, T. T.; Chang., J. P. *Appl. Phys. Lett.* **2005**, *87*(1), 011907/1–11907/3.
(4) Van, T. T.; Bargar, J. R.; Chang., J. P. *J. Appl. Phys.* **2006**, *100*(2), 023115/1–023115/.
(5) Toriumi, A.; Kita, K. *Dielectric Films for Advanced Microelectronics*; Baklanov, M.; Green, M.; Maex, K., Eds.; John Wiley & Sons: Chichester, U.K., 2007.
(6) Wilk, G. D.; Wallace, R. M.; Anthony, J. M. *J. Appl. Phys.* **2000**, *87*(1), 484–492.
(7) Tomida, K.; Kita, K.; Toriumi, A. *Appl. Phys. Lett.* **2006**, *89*(14), 142902/1–142902/3.
(8) Ho, M.-Y.; Gong, H.; Wilk, G. D.; Busch, B. W.; Green, M. L.; Lin, W. H.; See, A.; Lahiri, S. K.; Loomans, M. E.; Raisanen, P. I.; Gustafsson, T. *Appl. Phys. Lett.* **2002**, *81*(22), 4218–4220.
(9) Cho, M.-H.; Chang, H. S.; Cho, Y. J.; Moon, D. W.; Min, K.-H.; Sinclair, R.; Kang, S. K.; Ko, D.-H.; Lee, J. H.; Gu, J. H.; Lee, N. I. *Appl. Phys. Lett.* **2004**, *84*(4), 571–573.
(10) Wang, T.; Ekerdt, J. G. *Chem. Mater.* **2009**, *21*(14), 3096–3101.
(11) Park, T. J.; Kim, J. H.; Jang, J. H.; Na, K. D.; Hwang, C. S.; Yoo, J. H. *Electrochem. Solid-State Lett.* **2008**, *11*(5), H121–H123.
(12) Majumder, P.; Jursich, G.; Takoudis, C. *J. Appl. Phys.* **2009**, *105*(10), 104106/1–104106/6.

Published on Web 05/18/2010

different structure have different crystallization behavior; films deposited by alternating Hf and Al cycles in a 2:1 ratio are found to have a lower degree of crystallization than films deposited by alternating in a 4:2 ALD cycle ratio, even though the ratios of Hf and Al are the same.[13] The separation distance between Er ions in Y_2O_3 is also a critical parameter to fabricate high-performance fiber amplifiers.[14,15] In these cases, the ALD-grown ternary system is neither a nanolaminate with clear layer interface nor a homogeneous mixture. And the distribution of the incorporated material is a critical factor determining the film property. Therefore, it is important to understand how the incorporated material is intermixed with the host.

In this paper, we use the La-HfO_2 system to study how the two materials might be intermixed. HfO_2 is one of the most promising high-k dielectric materials to replace conventional SiO_2 as its physical limit (2 nm) has been reached.[16] But there are some issues remaining to be solved. One of them is HfO_2 crystallizes after annealing at a relatively low temperature (500 °C).[17] Although crystallized HfO_2 has a higher dielectric constant, stabilizing HfO_2 in its amorphous phase is more desirable, because the grain boundaries in the polycrystalline films serve as a charge leakage pathway and the coexistence of cubic, tetragonal, and monoclinic phases in the polymorphs results in different dielectric constants among different regions of the devices.[16,18,19]

Unlike nanolaminate or superlattice structures,[20,21] it is more difficult to characterize the periodicity of these ALD-grown films because the repeated structures can be extremely thin and the films are amorphous. The incorporation concentration has to achieve a certain level to alter the film property. With respect to ALD-grown La-incorporated HfO_2 films, the x value has to be 6 and 3 in order for a 10 nm film to remain amorphous after 800 and 900 °C annealing, respectively.[10] The growth rates of HfO_2 and La_2O_3 are 0.8 and 0.5 Å/cycle, respectively; for a film at a functionally reasonable incorporation level, one [xHf+1La] sequence is thinner than 6 Å. Therefore any compositional variations will be averaged in normal 45° take off angle X-ray photoelectron spectroscopy (XPS) analysis, since the electron effective attenuation lengths of Hf 4f and La 3d photoelectrons excited by Al $K\alpha$ is calculated to be 26.7 and 16.6 Å, respectively, at a 45° take off angle.[22] Cross sectional transmission electron microscopy, using the instrument at our disposal, a JEOL 2010F, is also unable to characterize such a small periodically distributed difference.

Angle-resolved X-ray photoelectron spectroscopy (AR-XPS) has been shown to be a powerful nondestructive tool to determine the thickness, fractional coverage and concentration depth profile for ultrathin films.[23−25] The XPS signal from the bulk material that is detected at the sample surface is given by

$$I = I_0 \exp(-d/\lambda \sin\theta) \quad (1)$$

Lambda, λ, is the effective attenuation length (EAL),[22] and a more detailed discussion about EAL is reported elsewhere.[26,27] The angle (θ) between the analyzer and the sample surface is defined as the take off angle. At small take off angles, only photoelectrons from the near surface region are detectable.[25] Although the periodicity of ALD grown La-HfO_2 system is smaller than the EAL, at glancing take off angles, the abrupt presence of the first few $HfLa_xO_y$ layers is expected to be detectable by using the AR-XPS technique.

Ellipsometry is another nondestructive analytical method that can characterize both the microstructure and electronic structure of solids by measuring the change in polarized light upon light reflection from a sample.[28] The complex dielectric function is given by, $\varepsilon = \varepsilon_1 + i\varepsilon_2$, where ε_1 and ε_2 are the real and imaginary parts, respectively. For a thin film, the dispersion of its complex dielectric function, which can be determined from ellipsometry, is strongly connected to the film density.[29] In the process of our previous study concerning the amorphous stabilization phenomena of ALD-grown La-HfO_2 systems, we noticed that the thickness reduction for the films after annealing is correlated to the x value in the [xHf + 1La] sequences. Thus ellipsometry can be used as another technique to explore the relationship between HfO_2:La_2O_3 ALD cycle ratio and film structure.

2. Experimental Section

Film Deposition. Samples were deposited on n-Si(100) substrates at 250 °C using tetrakis (ethylmethylamino) hafnium Hf-[$N(CH_3)(C_2H_5)]_4$, tris[*N*,*N*-bis(trimethylsilyl)-amino] lanthanum

(13) Katamreddy, R.; Inman, R.; Jursich, G.; Soulet, A.; Takoudis, C. *Acta Materialia* **2008**, *56*(4), 710–718.
(14) Van, T. T.; Hoang, J.; Ostroumov, R.; Wang, K. L.; Bargar, J. R.; Lu, J.; Blom, H.-O.; Chang, J. P. *J. Appl. Phys.* **2006**, *100*(7), 073512/1–073512/7.
(15) Desurvire, E. *Erbium-Doped Fiber Amplifiers*; Wiley: New York, 1994.
(16) Wilk, G. D.; Wallace, R. M.; Anthony, J. M. *J. Appl. Phys.* **2001**, *89* (10), 5243–5275.
(17) Gusev, E. P.; Cabral, C.; Copel, M.; D'Emic, C.; Gribelyuk, M. *Microelectron. Eng.* **2003**, *69*(2−4), 145–151.
(18) Mommer, N.; Lee, T.; Gardner, J. A. *J. Mater. Res.* **2000**, *15*(2), 377–381.
(19) Zhao, X.; Vanderbilt, D. *Phys. Rev. B* **2002**, *65*(23), 233106/1–233106/4.
(20) Cho, M.-H.; Roh, Y. S.; Whang, C. N.; Jeong, K.; Choi, H. J.; Nam, S. W.; Ko, D.-H.; Lee, J. H.; Lee, N. I.; Fujihara, K. *Appl. Phys. Lett.* **2002**, *81*(6), 1071–1073.
(21) Adelmann, C.; Kesters, J.; Opsomer, K.; Detavernier, C.; Kittl, J. A.; Van Elshocht, S. *Appl. Phys. Lett.* **2009**, *95*(9), 091911/1–091911/3.
(22) Powell, C. J.; Jablonski, A. *NIST Electron Effective-Attenuation-Length Database-Version 1.0*; National Institute of Standards and Technology: Gaithersburg, MD, 2001.
(23) Champaneria, R.; Mack, P.; White, R.; Wolstenholme, J. *Surf. Interface Anal.* **2003**, *35*(13), 1028–1033.
(24) Mack, P.; White, R. G.; Wolstenholme, J.; Conard, T. *Appl. Surf. Sci.* **2006**, *252*(23), 8270–8276.
(25) Chang, J. P.; Green, M. L.; Donnelly, V. M.; Opila, R. L.; Eng, J., Jr.; Sapjeta, J.; Silverman, P. J.; Weir, B.; Lu, H. C.; Gustafsson, T.; Garfunkel, E. *J. Appl. Phys.* **2000**, *87*(9 Pt.1), 4449–4455.
(26) Jablonski, A.; Powell, C. J. *J. Electron Spectrosc. Relat. Phenom.* **1999**, *100*, 137–160.
(27) Vitchev, R. G.; Defranoux, Chr.; Wolstenholme, J.; Conard, T.; Bender, H.; Pireaux, J. J. *J. Electron Spectrosc. Relat. Phenom.* **2005**, *149*(1−3), 37–44.
(28) Fujiwara, H. *Spectroscopic Ellipsometry: Principles and Applications*; Wiley: West Sussex, U.K., 2007.

$La[N(SiMe_3)_2]_3$ and H_2O; the precursors were held at 85, 150, and 25 °C, respectively. A detailed film deposition procedure is reported elsewhere.[10] The adsorption of $Hf[N(CH_3)(C_2H_5)]_4$ has been proved to be a self-limiting process at 250 °C.[30] The ALD of La_2O_3 using the same precursor is also reported at the same growth temperature.[31] To remove the native oxide from Si(100), we etched the Si substrates in a 2% HF solution for 30 s, rinsed them in deionized water for 20 s, and then dried them with flowing He. One cycle consists of precursor dosing for 1.5 s, a 15 s purge with Ar, water dosing for 0.05 s, and a 25 s purge with Ar. The ALD system consists of a custom built, hot wall stainless steel vessel that is connected to an XPS chamber. Substrate samples are 2×2 cm^2 and are mounted on a molybdenum stage that can be moved in situ between the ALD chamber and the analysis chamber. The ALD chamber is pumped by a turbomolecular pump to a base pressure of 5×10^{-6} Torr and is connected to the XPS analysis chamber through a load lock with a base pressure of 2×10^{-7} Torr. The growth rate of HfO_2 and La_2O_3 in our ALD system is 0.8 and 0.5 Å/cycle, respectively. The La-incorporation is achieved by growing HfO_2 and La_2O_3 alternately; x cycles of HfO_2 are grown plus one cycle of La_2O_3, and then this sequence is repeated n times to achieve the desired thickness. Films are referenced using $[x\text{Hf} + 1\text{La}] \times n$. Film growth always ends with an xHf cycle to minimize adsorption of ambient CO_2 and H_2O on the La_2O_3.[32,33] All films are confirmed to be 10 ± 0.4 nm by ellipsometry. Note an ALD layer does not imply a complete monolayer of a particular material, and we refer to an ALD layer as the amount deposited in a single ALD cycle.

Cross-Sectional Transmission Electron Microscopy (TEM) and Atomic Force Microscopy (AFM). TEM images for two as-deposited samples with high and low La-incorporation levels were acquired using a JEOL 2010F high-resolution transmission electron microscope with a field emission gun operated at 200 kV. The cross sections were prepared using a dicing saw followed by focused ion beam (FIB) milling. The FIB milling was conducted with a FEI Strata DB235 dual beam SEM/FIB system, which combines a scanning electron microscope (SEM) with a Ga ion beam source for nanoscale cutting. The AFM images of selected samples are acquired using a Veeco Dimension 3100 Scanning Probe Microscope operated at tapping mode, 1 μm^2 scan size and 0.5 Hz scan rate.

X-ray Photoelectron Spectroscopy (XPS). XPS is conducted using a Physical Electronics 5500 XPS system with a Mg $K\alpha$ source at 1253.6 eV and a Al $K\alpha$ source at 1486.6 eV. The base pressure of the XPS chamber is 1×10^{-9} Torr. The angle between the X-ray source and the photoelectron analyzer is 54.7°. The normal take off angle (between the analyzer and the sample surface) is 45°, at which XPS is normally performed using the Al source to acquire the averaged overall atomic percentage of Hf, La, and Si. AR-XPS is achieved by tilting the sample in a set of planes perpendicular to the plane defined by the X-ray source and the analyzer. The sample position has been calibrated so that the tilt axis crosses the intersection point of the X-ray and the analyzer. La 3d, Hf 4f, and O 1s photoelectrons are recorded in AR-XPS experiments. O 1s, instead of Hf 4f, is used as the reference for La 3d because the ratio of (La 3d)/(Hf 4f) varies too much with different take off angles, diminishing the features that can be observed at near-grazing take off angles. All XPS measurements are conducted in situ for as-deposited samples.

Ellipsometry. Ellipsometry is conducted using a J.A. Woollam M2000 Spectroscopic Ellipsometer. The ellipsometric data are interpreted using a Cauchy model and an effective medium approximation (EMA) model. The measurements are performed at 1.24−6.5 eV. Cauchy model fitting is limited to 1.24−3.3, 1.24−3.3, and 1.24−3.5 eV for HfO_2, $[x\text{Hf} + 1\text{La}] \times n$, and La_2O_3 films, respectively. The Cauchy model is used to establish film thickness for as-deposited and annealed films. The EMA model is used to interpret changes in the complex dielectric function as HfO_2, La_2O_3 and voids are combined in as-deposited films. In applying the EMA model, the solid component is modeled as a separate EMA material, composed of HfO_2 and La_2O_3 (with Si impurities) with known parameters, i.e., volume fraction and complex dielectric function. The complex dielectric function ($\varepsilon = \varepsilon_1 + i\varepsilon_2$) of 100 nm thick HfO_2 and La_2O_3 (with Si impurities) is measured to describe optical properties of the two constituents in the solid using the point-by-point data inversion method available in the J. A. Woollam software package. The EMA model describing the whole film is modeled by fitting the void fraction and the film thickness at 1.24−5.3 eV. The quality of the fit was assessed by evaluation of the mean-squared error (MSE) function:

$$\mathrm{MSE} = \frac{1}{2N - M} \times \sum_{i=1}^{N} \left[\left(\frac{\psi_i^{\mathrm{mod}} - \psi_i^{\mathrm{exp}}}{\sigma_{\psi,i}^{\mathrm{exp}}} \right)^2 + \left(\frac{\Delta_i^{\mathrm{mod}} - \Delta_i^{\mathrm{exp}}}{\sigma_{\Delta,i}^{\mathrm{exp}}} \right)^2 \right] \quad (2)$$

where N represents the number of (Ψ, Δ) experimental pairs, M is the number of variable parameters in the model, and σ are the standard deviations on the experimental data points. The resultant MSE values from the Cauchy model are <2. The MSE values for the EMA model are presented in Section 3.2.

3. Results and Discussion

In this work, the films are composed of three components, HfO_2, La_2O_3, and SiO_x impurities; Si impurities come from the trimethylsilyl-amino ligands on the La precursor. A periodic structure with repeated HfO_2 separated by La-rich layers is expected due to the ALD layer-by-layer growth process. But the cross-sectional TEM images of two 10 nm samples with high and low La-incorporation levels, $[3\text{Hf} + 1\text{La}] \times 41$ (Figure 1a) and $[9\text{Hf} + 1\text{La}] \times 14$ (Figure 1b), do not show any contrast variation. Both films appear homogeneous with an amorphous structure. This is because the thickness for a $[9\text{Hf} + 1\text{La}]$ sequence is extremely thin (<1 nm) and one ALD La_2O_3 layer does not form a complete monolayer. Electron energy loss spectroscopy (EELS) mapping also does not work because both Hf and La are heavy atoms and the beam size for our system is 1 nm. Similarly, the atomic concentrations of Hf and La do not vary with increasing sputtering time in XPS depth-profiling analysis since the EALs of Hf 4f and La 3d photoelectrons are longer than the thickness of the repeated structures.

(29) Kimura, H. *Mater. Res. Soc. Symp. Proc.* **2000**, *621*, Q5.7.1–Q.75.7.6.
(30) Kukli, K.; Ritala, M.; Sajavaara, T.; Keinonen, J.; Leskela, M. *Chem. Vap. Deposition* **2002**, *8*(5), 199–204.
(31) He, W.; Schuetz, S.; Solanki, R.; Belot, J.; McAndrew, J. *Electrochem. Solid-State Lett.* **2004**, *7*(7), G131–G133.
(32) Suzuki, M.; Kagawa, M.; Syono, Y.; Hirai, T. *J. Cryst. Growth* **1991**, *112*(4), 621–627.
(33) De Asha, A. M.; Critchley, J. T. S.; Nix, R. M. *Surf. Sci.* **1998**, *405* (2/3), 201–214.

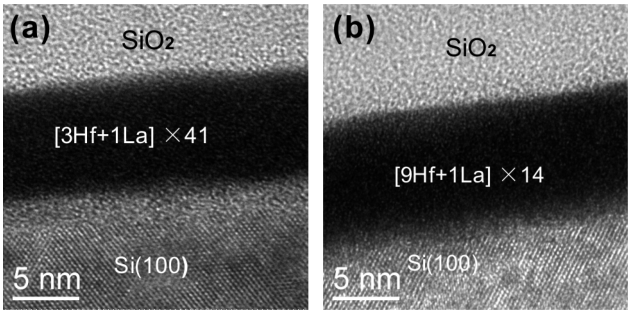

Figure 1. Cross-sectional TEM images for two as-deposited samples at (a) high La-incorporation level, [3Hf+1La] × 41; and (b) low La-incorporation level, [9Hf+1La] × 14. Both samples are homogeneous in TEM.

To overcome the difficulties in direct analysis methods such as TEM and normal XPS depth-profiling, we used AR-XPS and ellipsometry to reveal the existence of periodic structures. In situ AR-XPS measures the La 3d, Hf 4f, and O 1s signal at different take off angles, which define the sampling depth. The (La 3d)/(O 1s) and (Hf 4f))/(O 1s) signal intensity ratios are expected to vary depending on the sampling depth. Through AR-XPS analysis, a unique feature associated with $HfLa_xO_y$ layers separated by HfO_2 layers in the near surface region of the films is developed at grazing take off angles for films with real periodic structures. The take off angles marking these features can be used to calculate the relative intermixing degree of the two metal ions. Through ellipsometry analysis, the structural difference of as-deposited [xHf + 1La] films with different x values is characterized by using a model assuming the film is composed of solids and voids. The void fraction shows an abrupt decrease when the number of Hf cycles is $x = 3$, which further illustrates a $HfLa_xO_y$−HfO_2−$HfLa_xO_y$ structure and it takes a finite number of Hf cycles to recover deposition of HfO_2.

3.1. Angle-Resolved XPS. The EAL is kinetic-energy-dependent,[34] therefore the Mg Kα source at 1253.6 eV, instead of the Al Kα source, is used in AR-XPS analysis to reduce the EAL and probe a thinner region near the free sample surface. A 10 nm as-deposited [4Hf + 1La] × 32 sample is used to illustrate the approach. Intense La 3d and Hf 4f peaks are found at the normal detection geometry ($\theta = 45°$) in panels a and b in Figure 2, respectively. The unit of intensity is in counts per second (cps) so that the absolute values of the peak intensity can be compared between Hf 4f and La 3d signals at the same take off angles. As the take off angle decreases, the Hf 4f peak intensity decreases because less of the total film is sampled, but the Hf 4f signal is always detectable (Figure 2 c) because the film is capped with 4 Hf cycles after the final La cycle. Meanwhile, the La 3d signal completely disappears at $\theta = 2°$ (Figure 2d), which means at a sampling depth corresponding to $\theta = 2°$ the film is composed wholly of HfO_2. At $\theta = 3°$ (or 4°), the La 3d peak starts to appear as the sampling depth is large enough to reach the first $HfLa_xO_y$ layer.

(34) Seah, M. P.; Dench, W. A. *Surf. Interface Anal.* **1979**, *1*, 2–11.

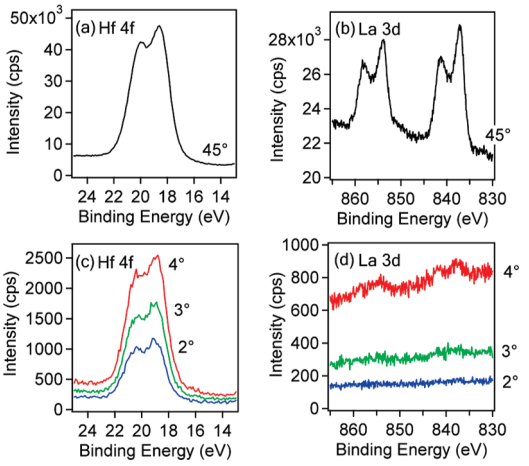

Figure 2. X-ray photoelectron spectra of Hf 4f and La 3d of a 10 nm as-deposited [4Hf+1La] × 32 sample at (a, b) normal 45° take off angle; and at (c, d) near-grazing take off angles.

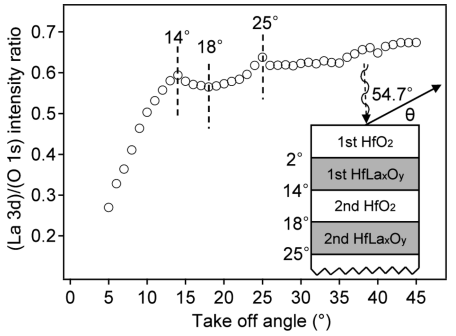

Figure 3. (La 3d)/(O 1s) photoelectron intensity ratio of a 10 nm as-deposited [4Hf+1La] × 32 sample. $14° \le \theta \le 18°$ and $18° \le \theta \le 25°$ represent the second HfO_2 and $HfLa_xO_y$ layer from the sample surface, respectively.

As the take off angle is gradually increased from near grazing to 45°, the periodicity of a [4Hf + 1La] film will become explicit as EAL × sin θ encounters the first few $HfLa_xO_y$ layers. Figure 3 shows the (La 3d)/(O 1s) photoelectron intensity ratio of a 10 nm as-deposited [4Hf + 1La] × 32 sample. The curve can be divided into four sections corresponding to different depths in the film. When the take off angle is larger than 2° and smaller than 14°, the (La 3d)/(O 1s) ratio increases rapidly with increasing take off angle, because $2° < \theta < 14°$ corresponds to a sampling depth range that fully includes the first HfO_2 layer from the top and gradually includes the first $HfLa_xO_y$ layer. Within the $2° < \theta < 14°$ range of angles, more and more La from the first $HfLa_xO_y$ layer is sampled, while the O being sampled remains relatively constant since both HfO_2 and La_2O_3 contain O atoms. When the take off angle is increased from 14 to 18° ($14° \le \theta \le 18°$), the curve decreases slowly, because the sampling depth includes the entire first HfO_2 and $HfLa_xO_y$ layers, and gradually includes the second HfO_2 layer from the top. Before detecting the second $HfLa_xO_y$ layer, the amount of La being sampled remains constant while more and more O from the second HfO_2 layer is sampled. For take off angles between 18 and 25° ($18° \le \theta \le 25°$), the sampling depth fully includes the first HfO_2 and $HfLa_xO_y$

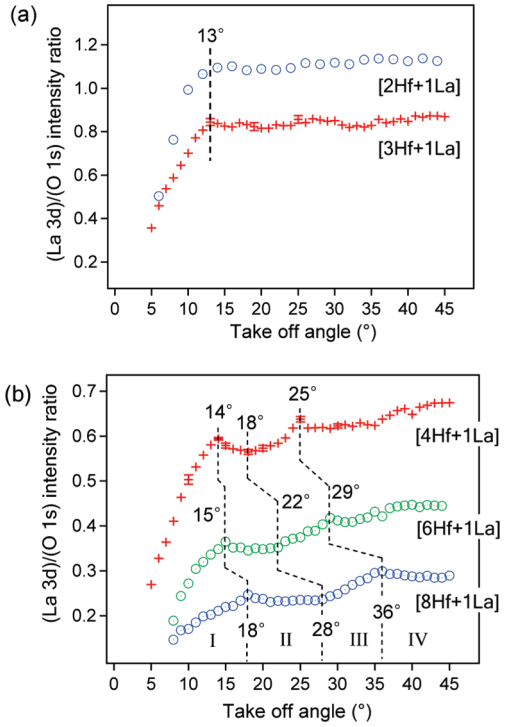

Figure 4. (La 3d)/(O 1s) photoelectron intensity ratio of a set of [xHf+1La] samples. (a) When x = 2, 3, the films are more like homogeneous mixtures; (b) when x = 4, 6, 8, the existence of an $HfLa_xO_y$–HfO_2–$HfLa_xO_y$ structure is confirmed by the features marked as sections I, II, and III.

layers and the second HfO_2 layer and starts to gradually include the second $HfLa_xO_y$ layer. The La from the second $HfLa_xO_y$ layer makes the (La 3d)/(O 1s) intensity ratio increase again, but this increase (and rate of increase) is not as big as that for $2° < \theta < 14°$ because La from the first $HfLa_xO_y$ layer is always being sampled. When the take off angle is beyond 25° ($\theta > 25°$), the sampling depth is too deep and the periodicity is averaged for our particular detector.

Applying the same AR-XPS characterization method to a set of 10 nm [xHf + 1La] samples, where x = 2, 3, 4, 6, and 8, a parallel comparison is acquired, illustrating how La is distributed in the growth direction. For x = 2 and 3, only the emergence of the first $HfLa_xO_y$ layer can be observed (Figure 4a), ceasing at θ = 13°. After that, the [2Hf + 1La] sample shows no periodicity under AR-XPS analysis, indicating a homogeneous film. The [3Hf + 1La] sample starts to show some variations, but compared with the noticeable feature of the [4Hf + 1La] sample in Figure 4b, the [3Hf + 1La] sample is more like a homogeneous film. All three films with lower La incorporation levels (x = 4, 6, 8) show the same trends in Figure 4b, i.e., section I , the first $HfLa_xO_y$ layer emerging through the top (first) HfO_2 layer; section II, the second La free HfO_2 layer; section III, the second $HfLa_xO_y$ layer; and section IV, the periodicity is averaged. Different sections show up at larger take off angels for films with a larger HfO_2:La_2O_3 ALD cycle ratio, which is caused by thicker La-free HfO_2 layers separating the $HfLa_xO_y$.

To check the reproducibility of this AR-XPS experiment, we conducted five measurements at seven different

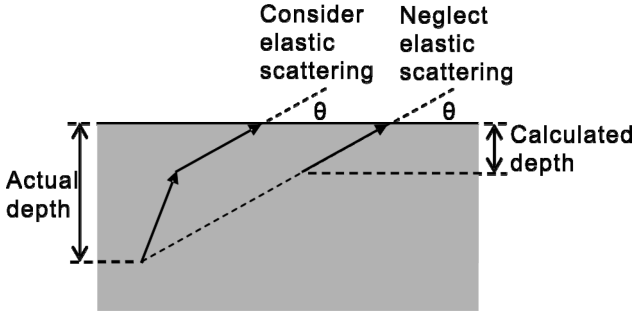

Figure 5. Schematic illustration of elastic scattering at small take off angles. Photoelectrons from a deeper depth may make their way to the sample surface through a shortcut caused by elastic scattering.

take off angles (10, 14, 15, 18, 20, 25, 30°) of the [4Hf + 1La] sample to acquire the standard deviation values, which are marked as the error bars at the corresponding data points in Figure 4b. As the La 3d signal noise-to-signal ratio is largely reduced at larger take off angles, the standard deviation values are small after 14° and the error bars at 14, 18, and 25° are much smaller than the maximum and minimum values defining the beginnings and endings of section II and III. Thus the existence of a periodic structure in ALD grown La-HfO_2 films is confirmed qualitatively by the features marked by section II and III in Figure 4b. For the [3Hf + 1La] sample (Figure 4a) to display periodicity, similar section II and III features should appear at 13−25° because any repeated La-free HfO_2 layer, if it exists, has to be thinner than that in the [4Hf + 1La] sample. The standard deviations for the measured ratios were checked at 13, 19, and 25° and are shown in Figure 4a. The changes in the intensity ratios between 13 and 25° are too close to the standard deviations to permit assigning section II and III features, implying tha the [3Hf + 1La] sample is more like a homogeneous film. Thus x has to be larger than 3 for La-free HfO_2 interval layers to start forming since [4Hf + 1La] is the lowest HfO_2: La_2O_3 ALD cycle ratio for the feature marked by sections II and III in Figure 4b start to develop.

To acquire a quantitative comparison among the three samples in Figure 4b, the National Institute of the Standards and Technology (NIST) database is used to calculate the practical EALs.[22] The product of the practical EAL and the sine of the take off angle equals to the depth normal to the surface from which a specific layer starts or ends, corresponding to a marked take off angle in Figure 4b. Sections II and III are the most informative part of the curves. Within section I, the take off angle is too small and the elastic scattering effect is not negligible so photoelectrons may escape from the surface by an additional path,[35] as shown in Figure 5. The elastic scattering effect is pronounced for photoelectrons produced at deeper depths. This is another contributing factor for the initial (La 3d)/(O 1s) increase in section I. O 1s, with a smaller binding energy compared with La 3d, results in photoelectrons with a bigger kinetic energy,

(35) Kimura, K.; Nakajima, K.; Conard, T.; Vandervorst, W. *Appl. Phys. Lett.* **2007**, *91*(10), 104106/1–104106/3.

Table 1. Calculated EALs at the Three Take off Angles That Define Section II and III; Overlayer Film Thickness at Which the Corresponding EALs are Calculated

	θ (deg)								
	[4Hf + 1La]			[6Hf + 1La]			[8Hf + 1La]		
	14	18	25	15	22	29	18	28	36
EAL (Å)	7.76	7.62	7.45	7.72	7.51	7.37	7.62	7.39	7.26
overlayer film thickness (Å)	1.88	2.35	3.15	2.00	2.81	3.58	2.35	3.46	4.28
EAL × sin θ (Å)[a]	1.88	2.36	3.15	2.00	2.81	3.57	2.36	3.47	4.27

[a] value of EAL × sin θ represents the thickness from which the photoelectrons being detected come.

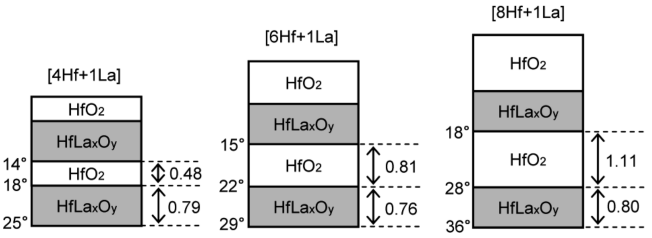

Figure 6. Pictorial presentation of the $HfLa_xO_y$−HfO_2−$HfLa_xO_y$ structure in [4Hf + 1La], [6Hf + 1La], and [6H f+ 1La] films. The relative thickness is calculated from the EAL × sin θ values in Table 1.

thus EAL(O 1s) > EAL(La 3d). Therefore the elastic scattering effect is more noticeable for O 1s at smaller take off angles, leading to more O detected from a deeper depth, which suppresses the (La 3d)/(O 1s) ratio at decreasing take off angles. The EAL depends on both take off angle and overlayer-film thickness, especially when the take off angle is near grazing,[22] so a set of practical EALs with different overlayer film thicknesses are calculated at different take off angles using the NIST database. A more reliable EAL can be determined by iterating and matching the value of EAL × sin θ and the overlayer film thickness at which the practical EAL is calculated. The final resultant EALs and their corresponding overlayer film thickness and EAL × sin θ at the three take off angles defining sections II and III are listed in Table 1 for the three samples.

The three values for EAL × sin θ of each sample can be regarded as the depths at which the La 3d signal shows the local compositional variation that defines section II and III. Note that these depth values do not reflect the real thickness, since the take off angle in section II and III are still very small, where the elastic scattering effect as shown in Figure 5 is not negligible. Elastic scattering contributes photoelectrons from deeper depths, which makes the calculated thicknesses smaller than what they should be. However, we still can use EAL × sin θ as a scale to predict the relative position of $HfLa_xO_y$ and La-free HfO_2 layers in the film.

For each sample, the differences of two adjacent EAL × sinθ values in Table 1 represent the second La free HfO_2 layer and the second $HfLa_xO_y$ layer from the top, respectively, as shown in Figure 6. The relative thickness of the second $HfLa_xO_y$ layer of all the three films is about 0.8 Å, indicating the vertical distance of La diffusion and/or dispersion is the same in all three samples. The calculated thickness of the second HfO_2 layer is about 0.5, 0.8, and 1.1 Å for the x = 4, 6, and 8, respectively. The relative thickness ratio of (HfO_2/$HfLa_xO_y$) is 0.61, 1.06, and 1.38 for [4Hf + 1La], [6Hf + 1La], and [8Hf + 1La], respectively.

From the ratios of the relative thicknesses of HfO_2 and $HfLa_xO_y$ for the three samples, we propose that one ALD layer of La_2O_3 interacts with more than two and less than three layers of HfO_2. The as-deposited film thickness measured by ellipsometry are [4Hf + 1La] × 32 (or 128Hf + 32La) = 10.2 nm; [8Hf + 1La] × 15 (or 120Hf + 15La) = 10.0 nm; and 125 cycles of HfO_2 = 10.1 nm, indicating the thickness contributed by La_2O_3 is negligible compared to HfO_2 for films with large x values. For the 4 ALD HfO_2 layers in a [4Hf + 1La] sequence, either 2 or 3 of them are intermixed with the underlying La_2O_3 according to the calculated relative thickness ratio. (Note that we consider only intermixing that happens with the underlying layer, because bidirectional intermixing involves layers both under and above the layer of interest, which gives the same result.) So the La-free HfO_2 is either two or one ALD layers and the ideal relative thickness ratio is 1.0 or 0.33, respectively. The value calculated by relative thickness is 0.61, which is in the middle. For the [6Hf + 1La] sample, the calculated relative thickness ratio value of 1.06 implies 6 ALD layers of HfO_2 are composed of 3 ALD layers of La free HfO_2 and 3 ALD layers of HfO_2 intermixing with La. For the [8Hf + 1La] sample, the calculated relative thickness ratio value of 1.38 is close to the ratio of 5 ALD layers of La-free HfO_2 and 3 ALD layers HfO_2 intermixing with La (5Hf/3Hf = 1.67). Therefore, more than two and less than three layers of HfO_2 intermix with La_2O_3.

3.2. Void Fraction by Ellipsometry. The film thickness, fit by the Cauchy model, decreases differently after the same annealing condition for different HfO_2:La_2O_3 ALD cycle ratios. The thickness of an 11.0 nm [1Hf + 1La] × 84 sample decreases to 8.8 nm after 900 °C 30 s annealing in a N_2 atmosphere; the absolute thickness decrease is 2.2 nm and the reduction is 20%. (A 1 nm SiO_2 interfacial layer forms during deposition[10] and the thicknesses reported in this paragraph include the interfacial layer.) But for films with larger x values, the thickness decrease is much smaller. An 11.2 nm [4Hf + 1La] × 32 sample and an 11.0 nm [8Hf + 1La] × 15 sample both decreased to 10.6 nm after 900 °C 30 s annealing in N_2 (6 and 4% thickness reduction, respectively). Finally, an 11.1 nm HfO_2 film grown by 125 cycles ($x \rightarrow \infty$) decreases to 10.7 nm after annealing at the same condition (4% reduction). The thickness reductions of pure HfO_2 and [xHf + 1La] with larger x values (4 and 8) in our study are close to HfO_2 films grown at 300 °C from a $HfCl_4$ precursor that have a reported density of 9.6 g/cm^3.[36] The density of a 10 nm HfO_2 film grown in this study was 9.9 g/cm^3, as measured by X-ray reflectometry (XRR). The thickness reduction

(36) Triyoso, D.; Liu, R.; Roan, D.; Ramon, M.; Edwards, N. V.; Gregory, R.; Werho, D.; Kulik, J.; Tam, G.; Irwin, E.; Wang, X. -D.; La, L. B.; Hobbs, C.; Garcia, R.; Baker, J.; White, B. E., Jr.; Tobin, P. *J. Electrochem. Soc.* **2004**, *151*(10), F220–F227.

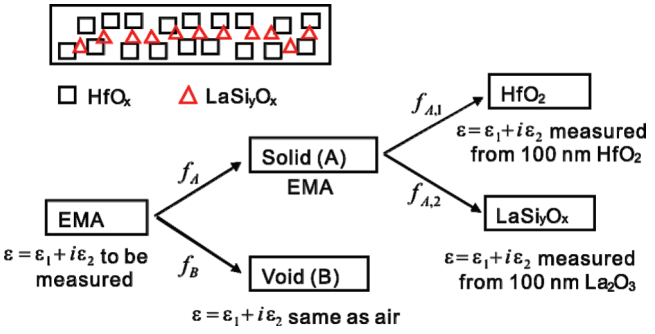

Figure 7. Schematic illustration of a film described by an EMA model, which incorporates a solid (material A) with its separate EMA model and voids (material B). Volume fractions f_A, f_B are fitted to the spectra; volume fractions $f_{A,1}, f_{A,2}$ are calculated from the measured atomic composition. The optical properties of HfO_2 and La_2O_3 are measured from two 100 nm thick samples.

of [1Hf+1La] × 84 in our study is even higher than HfO_2 grown at 200 °C in ref 36. that had a density of 8.8 g/cm^3. The thickness decrease differences between [xHf + 1La] with smaller and larger x values suggest that their atom packing arrangement may be different.

The Hf and La precursor ligands differ in size; Hf and La ions differ in both cation radii and coordination number, and the Hf−O and La−O bond lengths differ. So it is reasonable to expect different atom packing arrangements for the La-free HfO_2 and the $HfLa_xO_y$ regions. The packing arrangements determine the thickness decrease for films before and after annealing, as well as the density of the as-deposited films.

When a film is not dense, its complex dielectric function can be represented by the effective medium approximation (EMA) model.[37] The usual interpretation of the EMA theory is that small particles of one material are suspended in a matrix of the host material, voids and solid in this case. The use of void, with optical constants of empty space (or air), is simply a convenient way to raise or lower the dielectric constant of a known material to obtain the dielectric constant for the material of interest. The term should not be taken to imply the presence of small cavities, which could be seen with high-resolution microscopy.[37] In the Bruggeman EMA model, the complex dielectric function of ε is defined as in eq 3[38]

$$f_A \frac{\varepsilon_A - \varepsilon}{\varepsilon_A + 2\varepsilon} + f_B \frac{\varepsilon_B - \varepsilon}{\varepsilon_A + 2\varepsilon} = 0 \qquad (3)$$

where f_A and f_B are the volume fractions of each constituent material, and ε_A and ε_B are their complex dielectric functions. Herein we denote the solid component as A and voids as B. Material A can be described by another EMA model, which is composed of HfO_2 and La_2O_3 with Si impurities ($LaSi_yO_x$), as illustrated in Figure 7.

To describe the EMA model (solid A) that represents the solid part in the film, one needs the volume fractions

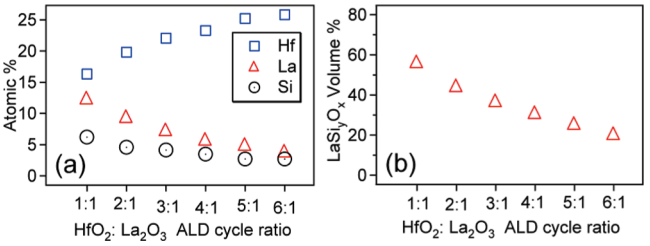

Figure 8. (a) Overall atomic percentage of Hf, La, and Si impurities; (b) and volume fraction of $LaSi_yO_x$ ($f_{A,2}$) in solids of a set of 10 nm as-deposited [xHf + 1La] films, where x = 1−6.

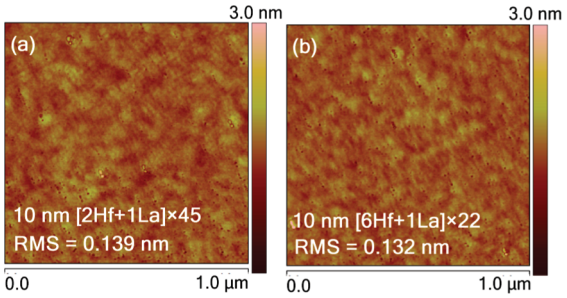

Figure 9. AFM images of as-deposited 10 nm (a) [2Hf + 1La] × 45 and (b) [6Hf + 1La] × 22 samples; the rms roughness is (a) 0.139 and (b) 0.132 nm.

of the two constituents in material A, $f_{A,1}$ and $f_{A,2}$, and their dielectric functions. A 100 nm HfO_2 film and a 100 nm La_2O_3 film (with 9.6% Si impurity) are deposited to determine the optical properties of HfO_2 and $LaSi_yO_x$. Knowing the density of amorphous HfO_2, La_2O_3 and SiO_2, $f_{A,1}$ and $f_{A,2}$ can be calculated by converting their atomic percentage calculated by XPS to the corresponding volume fractions. Here XPS is conducted using Al Kα at 1486.6 eV and a fixed 45° take off angle to acquire the averaged overall atomic percentage of Hf, La and Si in the bulk film. The atomic percentage is shown in Figure 8a and the volume fraction of $LaSi_yO_x$ ($f_{A,2}$) is shown in Figure 8b. Both the atomic percentage of La and Si and the volume fraction of $LaSi_yO_x$ decrease gradually with increasing HfO_2:La_2O_3 ALD cycle ratio.

Six 10 nm as-deposited (i.e., before annealing) samples with HfO_2:La_2O_3 ALD cycle ratios varying from 1:1 to 6:1 are characterized using the method described above. The fitting is performed for the 70° incident angle data, and at the range of 1.24−5.3 eV, or 234−1000 nm, which is much longer then the film thickness and sample roughness. As shown in images a and b in Figure 9, the root-mean-square (rms) roughness of as-deposited 10 nm [2Hf + 1La] × 45 and [6Hf + 1La] × 22 samples are 0.139 and 0.132 nm, respectively. The rms roughness of as-deposited 10 nm HfO_2 is 0.131 nm (image not shown). The samples have smooth surfaces without any distinguishable features, and the morphology does not change with different HfO_2:La_2O_3 ALD cycle ratios. Thus a simple three-phase model consisting of substrate/film(EMA)/ambient is used to fit the data since the surface morphology should not effect the ellipsometry result.

(37) Tompkins, H. G.; McGahan, W. A. *Spectroscopic Ellipsometry and Reflectometry: A User's Guide* John Wiley & Sons: New York, 1999.
(38) Aspnes, D. E.; Theeten, J. B.; Hottier, F. *Phys. Rev. B* **1979**, *20*(8), 3292–3302.

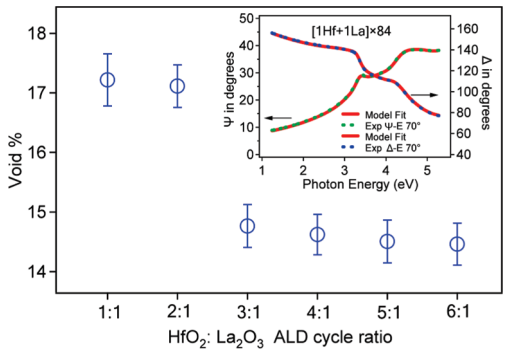

Figure 10. Void fractions of six as-deposited 10 nm [xHf+1La] films, where $x = 1-6$; inset, a typical ellipsometry spectrum of as-deposited 10 nm [1Hf + 1La] × 84.

The depolarization factor, which is a factor in the EMA model of the J. A. Woollam ellipsometry analysis software WVASE32 describing the shape of the constituents in the host matrix, is fixed to avoid correlation effects. A value of 1/3, corresponding to spherical shaped voids, is used. If a depolarization factor of 0 (needlelike) or 1 (columnar) is used, the calculated void fractions increase ~2% or decrease ~1% for each data point, respectively, whereas the shape of the resultant data curve remains the same. Because the void fraction calculated from the EMA model is more for comparison purposes in this study, the default depolarization factor of 1/3 (spherical) is used.

The calculated void fractions are shown in Figure 10 and a typical ellipsometry spectrum of 10 nm as-deposited [1Hf+1La] × 84 (the 1:1 sample) is presented as the inset. The resultant MSE values for the six samples are 5.9, 5.7, 5.9, 6.0, 6.2, and 6.3 from 1:1 to 6:1, respectively, indicating reasonably good fitting. Unlike Figure 8, the trend of the void fraction can be separated into two distinct parts. If the HfO_2:La_2O_3 ALD cycle ratio is 1:1 or 2:1, the void fraction is about 17.2%. When the ratio is 3:1 and above, the void fraction abruptly drops to 14.8% and then decreases very slowly.

Depolarization may affect the ellipsometry measurements due to incoherent reflections caused by excessive scattering, film thickness inhomogeneity, roughness, etc. Depolarization (or 1.0 - polarization) is mainly a concern when analyzing ellipsometry data from thick and/or inhomogeneous samples with large-scale nonuniformity. For the 6 samples with 1:1 to 6:1 HfO_2:La_2O_3 ALD cycle ratios, the measured depolarization curves from 1.24−5.3 eV are very close and are on the same order as the curve for Si(100) with a native oxide film (see Figure S1 in the Supporting Information). Thus depolarization affects all films similarly and there are no obvious differences between low and high x in the [xHf + 1La] films.

The La_2O_3 layer, which is not a complete monolayer, is mismatched dimensionally with HfO_2 and the partial layer is expected to have a different structure. Until Hf precursor molecules adsorb on a continuous HfO_2 film, the effective density of the incremental film that is added in each Hf cycle will be affected by the mismatch between HfO_2 and La_2O_3. The mismatch can also be explained by the retarded chemical adsorption process of the Hf precursor on a heterogeneous surface.[39] If $Hf[N(CH_3)(C_2H_5)]_4$ adsorbs on a Hf−OH surface (as in an ALD cycle of pure HfO_2), the distance between and the number density of −OH sites on the surface should be more uniform. But if $Hf[N(CH_3)(C_2H_5)]_4$ adsorbs on a heterogeneous (OH−Hf + La−OH) surface, the distance and the local number density of the −OH sites on the surface are more likely varied because of the different cation radii and coordination number of Hf and La, leading to a packing mismatch. This could affect the film structure and decreases the film density. The discontinuity in Figure 10 suggests that it takes three Hf cycles for HfO_2 to grow on itself, consistent with ~30% monolayer coverage/cycle of HfO_2 grown from the same Hf precursor.[40] After the third ALD layer of HfO_2 is deposited, the heterogeneous surface changes to a continuous Hf−OH surface, enhancing the adsorption of Hf precursors, which leads to a different structure with a different dielectric function and lower void fraction, compared with the La_2O_3−HfO_2 mixture during the deposition of the first three Hf cycles. Stated differently, one ALD layer of La_2O_3 interacts with more than two and less than three ALD layers of HfO_2 by forming a different structure, and the third ALD layer of HfO_2 is sufficient to terminate the interaction.

Both qualitative analysis of (La 3d)/(O 1s) ratios by AR-XPS and void fractions by ellipsometry indicate that La_2O_3 interacts with more than two and less than three ALD layers of HfO_2 in ALD grown La incorporated HfO_2 films. Thus if $x > 3$ for a [xHf + 1La] × n film, an $HfLa_xO_y$−HfO_2−$HfLa_xO_y$ structure does exist. Based on this, it is reasonable to conclude that the film is composed of repeated periodic $HfLa_xO_y$−HfO_2−$HfLa_xO_y$ structures because of the layer-by-layer growth mechanism of ALD, which supports what we proposed in the previous work.[10]

4. Conclusion

In summary, AR-XPS and ellipsometry are used to confirm the existence of a periodic structure of ALD grown La−HfO_2 films. More than two and less than three layers of HfO_2 interact with La_2O_3. From ellipsometry analysis, the interaction is composed of the first two ALD layers of HfO_2 mismatching with La_2O_3, and a third ALD layer that produces a continuous HfO_2 layer, which changes the film structure and lowers the void fraction. The quantitative analysis of (La 3d)/(O 1s) photoelectron intensity ratios acquired at near grazing AR-XPS take off angles indicates the one ALD layer of La_2O_3 interacts with more than two and less than three ALD layers of HfO_2; and the

(39) Kim, S. K.; Choi, G. J.; Kim, J. H.; Hwang, C. S. *Chem. Mater.* **2008**, *20*(11), 3723–3727.
(40) Consiglio, S.; Mo, R. T.; Tai, T. -L.; Krishnan, S. A.; O'Meara, D.; Wajda, C.; Chudzik, M. P. *ECS Trans.* **2007**, *6*(1), 167–177.

qualitative analysis illustrates at least 4 ALD layers of HfO_2, i.e., [4Hf + 1La], are necessary for La-free HfO_2 interval layers to exist in the film. This AR-XPS-ellipsometry complementary characterization method should be applicable to understand the intermixing phenomena in other ALD-grown periodic structure systems.

Acknowledgment. This work was supported by the National Science Foundation (Awards DMR-060646 and NNIN ECS-0335765).

Supporting Information Available: Degree of depolarization of 10 nm HfO_2, [xHf + 1La] (x = 2, 3, 4, 6, 8), and bare Si (PDF). This material is available free of charge via the Internet at http://pubs.acs.org.